Science of the Total Environment 839 (2022) 156130

Contents lists available at ScienceDirect

Science of the Total Environment

journal homepage: www.elsevier.com/locate/scitotenv

Pronounced increases in nitrogen emissions and deposition due to the historic 2020 wildfires in the western U.S.

Patrick C. Campbell [a,b,*], Daniel Tong [a,c], Rick Saylor [b], Yunyao Li [c], Siqi Ma [c], Xiaoyang Zhang [d], Shobha Kondragunta [e], Fangjun Li [d]

[a] Center for Spatial Information Science and Systems/Cooperative Institute for Satellite Earth System Studies, George Mason University, Fairfax, VA, USA
[b] Office of Air and Radiation, Air Resources Laboratory, National Oceanic and Atmospheric Administration, College Park, MD, USA
[c] Department of Atmospheric, Oceanic and Earth Sciences, George Mason University, Fairfax, VA, USA
[d] Geospatial Sciences Center of Excellence, Department of Geography & Geospatial Sciences, South Dakota State University, Brookings, SD, USA
[e] NOAA Satellite Meteorology and Climatology Division, NOAA Air Resources Laboratory, College Park, MD, USA

HIGHLIGHTS

- The 2020 "gigafires" contributed up to 83% of the total nitrogen emissions in the western U.S.
- The 2020 fire emissions led to a 78% increase in annual average nitrogen deposition in California.
- The average nitrogen deposition increases to California's forests are 6-12 times the critical load.

GRAPHICAL ABSTRACT

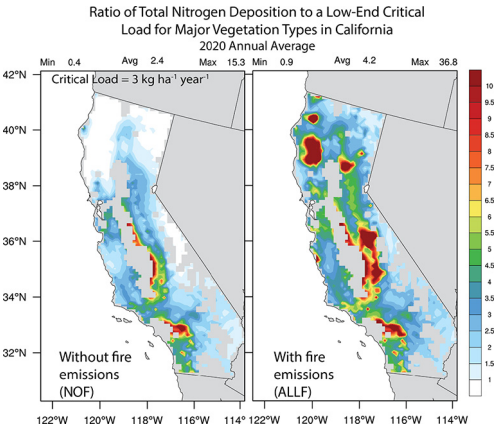

ARTICLE INFO

Editor: Jay Gan

ABSTRACT

Wildfire outbreaks can lead to extreme biomass burning (BB) emissions of both oxidized (e.g., nitrogen oxides; NO_x = NO + NO_2) and reduced form (e.g., ammonia; NH_3) nitrogen (N) compounds. High N emissions are major concerns for air quality, atmospheric deposition, and consequential human and ecosystem health impacts. In this study, we use both

Abbreviations: AMET, Atmospheric Model Evaluation Tool; ACC, Anomaly Correlation Coefficient; ACF, August Complex Fire; AOD, Aerosol Optical Depth; BB, Biomass Burning; EPA, Environmental Protection Agency; CAL FIRE, California Department of Forestry and Fire Protection; CASTNET, Clean Air Status and Trends Network; LADCO, Lake Michigan Air Directors Consortium; CO_2, Carbon Dioxide; CSN, Chemical Speciation Network; FED, Federal Land Manager Environmental Database; HNO_3^-, Nitric Acid Vapor; N, Nitrogen; WE-CAN, Western Wildfire Experiment for Cloud Chemistry, Aerosol Absorption, and Nitrogen; NO, Nitric Oxide; NO_2, Nitrogen Dioxide; NO_x, Nitrogen Oxides; NH_3, Ammonia; NO_3^-, Nitrate Ion; NH_4^+, Ammonium Ion; OxN, Oxidized Nitrogen; NHx, Reduced Nitrogen; PM25_TOT, Total $PM_{2.5}$; PM25_SO4, $PM_{2.5}$ Sulfate Ion; PM25_NO3, $PM_{2.5}$ Nitrate Ion; PM25_NH4, $PM_{2.5}$ Ammonium Ion; MONET, Model and Observation Evaluation Toolkit; TEMP2, 2-meter Temperature; Q2, 2-meter Water Vapor Mixing Ratio; WS10, 10-meter Wind Speed; WD10, 10-meter Wind Direction; TN, Total Oxidized and Reduced Nitrogen; FRP, Fire Radiative Power; GBBEPx, Blended Global Biomass Burning Emissions Product; $PM_{2.5}$, Fine Particulate Matter; GMU-WFS, George Mason University Wildfire Forecast System; WRF, Weather Research and Forecasting; CMAQ, Community Multi-Scale Air Quality Model; CONUS, Contiguous United States; CB6, Carbon Bond Version 6; CL, Critical Load; IMPROVE, Interagency Monitoring of Protected Visual Environments; NEI, National Emissions Inventory; NEIC, National Emissions Inventory Collaborative; NMB, Normalized Mean Bias; NME, Normalized Mean Error; IOA, Index of Agreement; RMSE, Root Mean Squared Error; MADIS, Meteorological Assimilation Data Ingest System; METAR, Meteorological Aerodrome Reports; MODIS, Moderate Resolution Imaging Spectroradiometer; VIIRS, Visible Infrared Imaging Spectrometer; SNPP, Suomi National Polar-orbiting Partnership; TOT_DEP TN, Total (Wet and Dry) Oxidized and Reduced Nitrogen Deposition; TOT_DEP NHx, Total (Wet and Dry) Reduced Nitrogen Deposition; TOT_DEP OxN, Total (Wet and Dry) Oxidized Nitrogen Deposition; JPSS1, Joint Polar-orbiting Satellite System 1; ALLF, All Fire Simulation; NOF, No Fire Simulation.

* Corresponding author at: 5830 University Research Ct, College Park, MD 20740, USA.
E-mail address: Patrick.C.Campbell@noaa.gov (P.C. Campbell).

http://dx.doi.org/10.1016/j.scitotenv.2022.156130
Received 7 March 2022; Received in revised form 16 May 2022; Accepted 17 May 2022
Available online 21 May 2022

Keywords:
2020 U.S. Wildfires
Biomass burning emissions
Nitrogen emissions
Nitrogen deposition
George Mason University-Wildfire Forecast System
WRF-CMAQ model

satellite-based observations and modeling results to quantify the contribution of BB to the total emissions, and approximate the impact on total N deposition in the western U.S. Our results show that during the 2020 wildfire season of August–October, BB contributes significantly to the total emissions, with a satellite-derived fraction of NH_3 to the total reactive N emissions (median ~ 40%) in the range of aircraft observations. During the peak of the western August Complex Fires in September, BB contributed to ~55% (for the contiguous U.S.) and ~ 83% (for the western U.S.) of the monthly total NO_x and NH_3 emissions. Overall, there is good model performance of the George Mason University-Wildfire Forecasting System (GMU-WFS) used in this work. The extreme BB emissions lead to significant contributions to the total N deposition for different ecosystems in California, with an average August – October 2020 relative increase of ~78% (from 7.1 to 12.6 kg ha^{-1} year^{-1}) in deposition rate to major vegetation types (mixed forests + grasslands/shrublands/savanna) compared to the GMU-WFS simulations without BB emissions. For mixed forest types only, the average N deposition rate increases (from 6.2 to 16.9 kg ha^{-1} year^{-1}) are even larger at ~173%. Such large N deposition due to extreme BB emissions are much (~6-12 times) larger than low-end critical load thresholds for major vegetation types (e.g., forests at 1.5-3 kg ha^{-1} year^{-1}), and thus may result in adverse N deposition effects across larger areas of lichen communities found in California's mixed conifer forests.

1. Introduction

Wildfires have been increasing in size (Westerling et al., 2006) and potentially in severity (Miller et al., 2009) over the past decades, especially in the western U.S. Wildfire emission outbreaks can lead to extreme emissions of both oxidized (e.g., nitrogen oxides; $NO_x = NO + NO_2$) and reduced forms (e.g., ammonia; NH_3) of nitrogen (N) compounds, where such N emissions are major concerns for air quality (e.g., ozone and fine particulate matter), atmospheric deposition, and the consequential human (Cascio, 2018; Reid et al., 2016) and ecosystem health impacts (Koplitz et al., 2021). Using data based on the Western Wildfire Experiment for Cloud Chemistry, Aerosol Absorption, and Nitrogen (WE-CAN) field campaign, Lindaas et al. (2021) found that reduced N compounds comprise a majority (39%–80%; median = 66%) of total measured reactive nitrogen emissions. These large emissions lead to shifts in the amount and forms of atmospheric N deposition to sensitive ecosystems that become ecologically significant and highly variable, particularly for select western U.S. (Geiser et al., 2010) and California ecosystems (Bytnerowicz et al., 2001; Fenn et al., 2000, 2008) within and surrounding major wildfire areas. Outside of major wildfires, the average annual N deposition in California ranges from about 1–45 kg ha^{-1} year^{-1} (Bytnerowicz et al., 2001); however, studies indicate significant contributions of wildfires to the total nutrient (nitrogen and sulfur) deposition (e.g., maximum ~30%) that have implications for tree growth and survival rates in some regions of the Northwest U.S. (Koplitz et al., 2021). Other studies show that locally enhanced N deposition (e.g., downwind of large urban areas or wildfires) to terrestrial and aquatic ecosystems can have negative ecological effects (e.g., biotic community changes and deleterious effects on sensitive organisms) when levels exceed the relatively low amounts of N deposition in the western U.S. (Fenn et al., 2003). There is also potential for differential effects of reduced vs. oxidized N deposition to varying vegetative habitats as well (van den Berg et al., 2015).

Previous studies of wildfire emissions and atmospheric N deposition are typically averaged over specific time periods that consist of many wildfire events/locations (e.g., the 2008–2012 period in Koplitz et al., 2021). This strategy may inherently dampen the effects of extreme wildfire events that are becoming ever more common in the western U.S. In this work, we analyze atmospheric N emissions and deposition resulting from the record-breaking 2020 wildfire season, which includes the extreme cluster wildfire event known as the "August Complex Fire" (ACF). The ACF originated as 38 separate fires started by lightning strikes on August 16–17, 2020, where the four largest fires, the Doe, Tatham, Glade, and Hull fires had combined and burned together by August 30. The ACF became the first "gigafire" event in modern history in California on October 5, defined as a blaze that burns at least 1 million acres. The total acres burned nearly doubled late on September 10, when the Elkhorn Fire merged with the ACF. The total area burned by ACF was 1,032,648 acres (~1% of the area of California) at the time it was extinguished on November 12, which is an area larger than the size of Rhode Island (https://inciweb.nwcg.gov/incident/6983/). Overall in 2020, California experienced 9917 incidents of multiple complex wildfires, which led to over 4 million acres burned and 10,488 structures destroyed (CAL FIRE, 2020).

The total biomass burning (BB) emission estimates for 2020 were historic in the western U.S., and were largely dominated by the ACF between August–October. The total carbon dioxide (CO_2) emissions due to the ACF were 27.7 million metric tons (Mmt) (https://ww2.arb.ca.gov/). There were also contributions from other very large "megafires" (at least 100,000 acres burned) during this period in the west including the Santa Clara Unit lightning complex (396,399 acres burned; 4.6 Mmt CO_2 emissions), Creek (379,882 acres burned; 13.8 Mmt CO_2 emissions), North Complex (318,777 acres burned; 10.9 Mmt CO_2 emissions), and Hennessey (305,352 acres burned; 3.5 Mmt CO_2 emissions) fires (https://ww2.arb.ca.gov/). Such historically large fires and their associated BB emissions lead to prominent amounts of N compounds that alter atmospheric chemistry, aerosol formation, and deposition (Li et al., 2021). Model results from Li et al. (2021) found that the record breaking wildfires and BB emissions in 2020 contributed to 81% of near-surface fine particulate matter ($PM_{2.5}$) concentrations during the U.S. Environmental Protection Agency (EPA)-defined air quality exceedances in the west. Many previous studies have evaluated BB emissions impacts on air quality and health (e.g., Johnston et al., 2012; Reid et al., 2016; Cascio, 2018; Li et al., 2021; Liu et al., 2021; O'Neill et al., 2021); however, there are only a few that assess the impacts of BB on both oxidized and reduced N emissions and their impacts on atmospheric deposition and ecosystem health (e.g., Koplitz et al., 2021), with no apparent studies covering these aspects for the 2020 ACF, extreme gigafire events in the U.S.

In this study, we analyze the 2020 U.S. wildfire season and focus on the ACF gigafire events to quantify the percent contribution of satellite-derived BB to the total emissions, evaluate the satellite-based wildfire model system used in the study, i.e., the George Mason University (GMU) Wildfire Forecast System (WFS; Li et al., 2021), and then use the GMU-WFS to approximate the impact of the 2020 BB emissions on total N deposition in the western U.S. We hypothesize and show that the extreme ACF gigafire events have prominent effects on the BB emissions of oxidized and reduced N and contribute significantly to the total (anthropogenic + BB source) emissions and atmospheric deposition in the western U.S.

2. Methods

2.1. Air quality modeling system

Here we employ the GMU-WFS, which is based on an offline-coupled Weather Research and Forecasting (WRF) model version 4.2 (Skamarock et al., 2019) meteorological output that is used to drive a chemical transport model known as the Community Multiscale Air Quality (CMAQ) model version 5.3.1 (U.S. EPA, 2020). The model resolution is 12 × 12 km, covers the contiguous U.S. (CONUS), and includes 35 vertical layers. While all model configuration details are not repeated here, we note that the Carbon

Bond Version 6 (CB6) gas-phase chemical mechanism (Luecken et al., 2019), Aero07 aerosol scheme (Pye et al., 2015; Xu et al., 2018), and aqueous chemistry (Fahey et al., 2017) are used in the CMAQ system. The reader is referred to Li et al. (2021) for the complete GMU-WFS configuration details and input data used in this study.

2.2. Model emissions inputs

The model emissions inputs may be the most influential input for chemical transport model predictions in any air quality prediction system (Matthias et al., 2018). This is indeed the case here for both the anthropogenic and BB emissions datasets, which have profound impacts on the model outputs. The anthropogenic base-year emissions are taken from the U.S. EPA National Emissions Inventory (NEI) Collaborative (NEIC) 2016v1 Emissions Modeling Platform, which is based on updated models and datasets applied to the U.S. EPA's NEI 2014 version 2 (NEIC, 2019). The base year's NEIC 2016v1 emissions are shifted to represent the 2020 prediction year's representative day-of-the-week in the GMU-WFS (Li et al., 2021).

There are advanced treatments of BB emissions and wildfire plume rise treatment in the GMU-WFS. The BB emissions are based on the Blended Global Biomass Burning Emissions Product (GBBEPx V3; Zhang et al., 2012, 2014). GBBEPx provides daily 0.1° × 0.1° global BB emissions for a number of gases and aerosols (NO_x, NH_3, carbon monoxide, sulfur dioxide, $PM_{2.5}$, Black Carbon, and Organic Carbon) derived from satellite-based Fire Radiative Power (FRP) values. It blends the fire observations from two sensors, including the Moderate Resolution Imaging Spectroradiometer (MODIS) on the NASA Terra and Aqua satellites, and the Visible Infrared Imaging Spectrometer (VIIRS) on the Suomi National Polar-orbiting Partnership (SNPP) and Joint Polar-orbiting Satellite System 1 (JPSS1) satellites. A global 1 km International Geosphere–Biosphere Programme (IGBP) land cover type is used to stratify land surface into tropical forests, extratropical forest, cerrado/woody savanna, and grassland/cropland. From these land cover types, emissions factors are assigned based on the Quick Fire Emissions Dataset (QFED; Darmenov and da Silva, 2013). The GBBEPx data are further processed to prepare model-ready emission datasets for the GMU-WFS. The original GBBEPx emissions input are at 0.1° × 0.1° degree globally (~ 10 × 10 km) and are close to the regional numerical simulation grid size (12 × 12 km; see Section 2.1). Thus, the GBBEPx re-gridding errors are minimal. The Sofiev plume rise scheme in GMU-WFS utilizes the FRP, planetary boundary layer height, and the Brunt-Vaisala frequency in the free troposphere to estimate fire injection height (Sofiev et al., 2012). The reader is referred to Li et al. (2021) for more details of GBBEPx and Li et al. (2020) for the Sofiev plume rise scheme used in the GMU-WFS for this study. We note that the GBBEPx performed well for other large wildfire events in California such as the Camp Fire (Li et al., 2020), and that, Li et al. (2020) found that GBBEPx together with the Sofiev plume rise scheme performed the best compared to different combinations of emissions datasets and plume rise algorithms in the GMU-WFS.

2.3. Simulation design, observations, and evaluation protocol

The simulation design in this paper consists of two sets of GMU-WFS runs, both with and without BB emissions. The first run (ALLF) includes all GBBEPx emissions from all fires (i.e., (wildfires, prescribed fires, and other BB sources), while the second run (NOF) is the same as in ALLF, except all types of GBBEPx emissions are excluded. Comparison of the GMU-WFS results from the ALLF and NOF runs quantify the impacts of all BB, wildfire, and prescribed fires on N deposition. The simulation period is run for the entire 2020 year including the historic summer wildfire season from August 01–October 31 over the CONUS domain, with initial conditions based on NOAA's well-established operational air quality forecasting system (https://airquality.weather.gov/). The Surface Weather Observations and Reports for Aviation Routine Weather Reports (METAR), collected by NCEP's Meteorological Assimilation Data Ingest System (MADIS) (https://madis.ncep.noaa.gov/madis_metar.shtml, last access: 5 April 2022), provide observations of 2-m temperature (TEMP2), 2-m specific humidity (Q2), and 10-m wind speed (WS10) and direction (WD10). Results from the ALLF case are further evaluated against the U.S. EPA AirNow network (https://www.airnow.gov/) for $PM_{2.5}$ and nitrogen dioxide (NO_2), and against the Chemical Speciation Network (CSN; https://www.epa.gov/amtic/chemical-speciation-network-csn) and the Interagency Monitoring of Protected Visual Environments (IMPROVE; http://vista.cira.colostate.edu/Improve/) network for total $PM_{2.5}$ and $PM_{2.5}$ sulfate, nitrate, and ammonium ions. The Clean Air Status and Trends Network (CASTNET) (https://www.epa.gov/castnet, last access 27 April 2022) provide weekly aggregated observations of nitrate and ammonium ion dry deposition. Full description of the GMU-WFS simulation design and additional model evaluations are found in Li et al. (2021).

The statistical measures used to evaluate the GMU-WFS meteorology and air quality predictions include the mean bias (MB), normalized mean bias (NMB), normalized mean error (NME), root-mean-square error (RMSE), anomaly correlation coefficient (ACC), Pearson's correlation coefficient (R), and index of agreement (IOA). Statistical measures such as R, NMB, and NME or RMSE provide measures of the associativity (i.e., correlation), bias, and accuracy, respectively, of the GMU-WFS modeled surface meteorology, chemistry, and deposition. The meteorological and chemical evaluations use the publicly available US EPA Atmospheric Model Evaluation Tool (AMET; Appel et al., 2011), NOAA/ARL Model and Observation Evaluation Toolkit (MONET; Baker and Pan, 2017), and NCAR Command Language (NCL; https://www.ncl.ucar.edu, last access: 5 April 2022).

3. Results

3.1. Relative contribution of nitrogen emissions from the 2020 wildfires

The average August–October 2020 mean FRP and associated NO_x emissions from GBBEPx show significant wildfire hotspots in California, particularly northern California (Fig. 1a-b). These hotspots are found in direct vicinity or just upstream of sensitive ecosystems in Central and Northern California (e.g. the Sierra Nevada Mountains). Because the GBBEPx emissions vary with different land use/vegetation types (Li et al., 2021), the NH_3/NO_x ratio shows spatial variability and ranges from 0.18–1.08 (Fig. 1c; average ~ 0.62 (i.e., 62%) for the western U.S., i.e., > 102°W). For further reference to the connection of GBBEPx and QFED land-use dependent species emission factors, Fig. S1 in the supporting information shows the QFED nitric oxide (NO) and NH_3 emissions as a function of different biomass types in California for an average of August–October 2020 (i.e. the ACF events). The majority of NO and NH_3 emissions are associated with the forest biomass type in California during the ACF events.

Furthermore, the ratio of the GBBEPx NH_3 emissions to the total reactive N (~ $NH_3/[NH_3 + NO_x]$*100%) is ~15%–52%, with a mean of ~37% and median of ~40% in the western U.S.(not shown). This is within the range of Lindaas et al. (2021) that showed reduced N compounds comprise a majority (39%–80%; median = 66%) of total reactive emissions during the 2018 Western wildfire Experiment for Cloud chemistry, Aerosol absorption and Nitrogen (WE-CAN; https://www2.acom.ucar.edu/campaigns/we-can; last access 09 May 2022), and suggests that the GBBEPx N emissions speciation is within the range of aircraft observations.

Comparison of the GBBEPx BB emissions to the total major (NEIC 2016v1 anthropogenic + GBBEPx BB) emissions sources over CONUS and just the western U.S. (> 102°W) indicates that BB contributes <20% (minimum ~3% during winter months) to the total NO_x and NH_3 emissions for most of the year; however, during the 2020 wildfire season of August–October, BB contributes significantly more to the total emissions (Fig. 1d and Table 1). During the peak of the ACF in

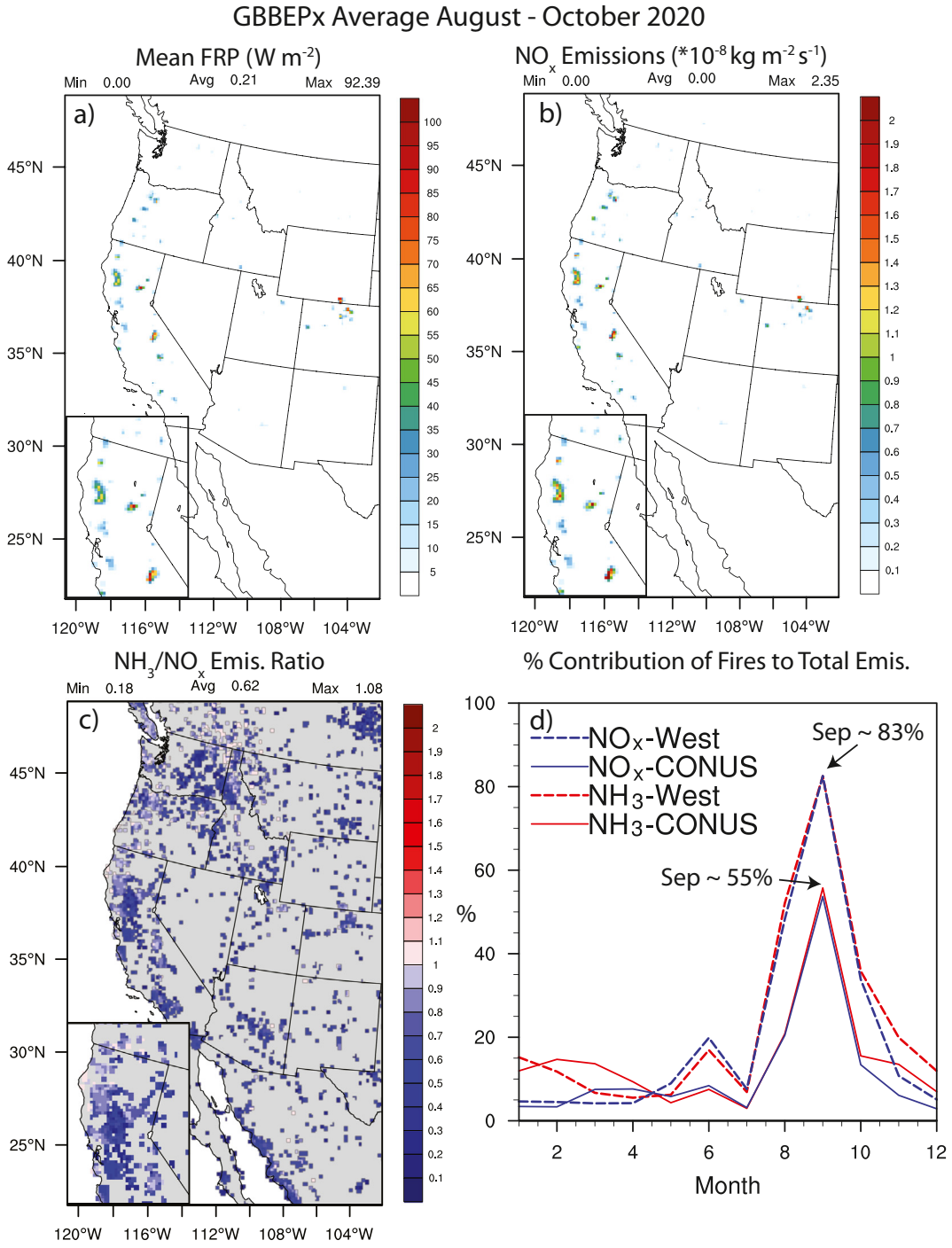

Fig. 1. Analysis of a)-c) spatial distribution of average August–October 2020 FRP, NO_x emissions, and NH_3/NO_x emissions ratio in the western U.S. (> 102°W and insert/zoomed-in N. California region), and d) 2020 monthly percent contribution of GBBEPx NO_x (blue) and NH_3 emissions (red) to total (NEI2016v1 + GBBEPx BB) emissions for entire CONUS domain (solid) and western U.S. only (dashed; > 102°W).

September, BB contributed to ~55% and ~ 83% of the total NO_x and NH_3 emissions in CONUS and the western U.S., respectively. These substantial fractions indicate the importance of enhanced BB emissions on the atmospheric N concentration and resulting deposition to surrounding ecosystems, particularly during the height of the ACF (gigafire) event in September 2020. Hence, while other months of the year 2020 are included in this paper (and in Supporting Information) for reference, the month of September is a main focus of the following analyses (Sections 3.2–3.4).

3.2. Evaluation of the GMU-WFS simulated meteorology, chemistry, and deposition

3.2.1. Meteorology evaluation

We first perform a spatial evaluation of wildfire-related meteorological variables predicted by the GMU-WFS, which include TEMP2, Q2, WS10, and WD10 against the MADIS/METAR network (Fig. 2).

The statistical GMU-WFS meteorological performances in Table 2 fall near or within typical model bias and error performance benchmarks for

Table 1
Total August – October 2020 NO_x and NH_3 GBBEPx and NEIC2016v1 emissions (in Tg) for the CONUS and western U.S. (> 102°W) regions. Supporting Table S1 shows similar monthly results for the entire 2020 year.

	NO_x (Tg)		NH_3 (Tg)	
	NEIC2016v1	GBBEPx	NEIC2016v1	GBBEPx
		August 2020		
CONUS	11.3	2.9	0.60	0.16
Western U.S.	2.8	2.6	0.14	0.14
		September 2020		
CONUS	10.2	11.8	0.38	0.48
Western U.S.	2.5	11.6	0.10	0.48
		October 2020		
CONUS	11.0	1.7	0.37	0.07
Western U.S.	2.6	1.4	0.10	0.06

Table 2
September 2020 average statistical metrics for the GMU-WFS simulated TEMP2, Q2, WS10, and WD10 compared against the MADIS/METAR network in the East and West U.S. regions.

Variable	East U.S. (< 100° W)				West U.S. (> 100° W)			
TEMP2	MB (°C)	RMSE (°C)	R	IOA	MB (°C)	RMSE (°C)	R	IOA
	−0.001	2.0	0.96	0.96	0.57	3.1	0.93	0.93
Q2	MB (g kg^{-1})	RMSE (g kg^{-1})	R	IOA	MB (g kg^{-1})	RMSE (g kg^{-1})	R	IOA
	−0.40	1.4	0.96	0.95	−0.43	1.5	0.87	0.86
WS10	MB (m s^{-1})	RMSE (m s^{-1})	R	IOA	MB (m s^{-1})	RMSE (m s^{-1})	R	IOA
	0.20	1.5	0.72	0.72	−0.54	1.9	0.71	0.69
WD10	MB (deg)	RMSE (deg)	R	IOA	MB (deg)	RMSE (m s^{-1})	R	IOA
	3.4	33.1	*n/a*	*n/a*	0.84	55.2	*n/a*	*n/a*

both relatively simple (e.g., East U.S.) and complex terrain (West U.S.) conditions (see Table 5–1 in LADCO, 2018). Supporting Fig. S2 also shows a statistical evaluation of the diurnal characteristics of GMU-WFS predicted TEMP2, Q2, and WS10 and WD10. Given the nuances of using typical statistical metrics to evaluate model wind directions (see *n/a* values in Table 2), Supporting Fig. S3a-S3b also show more robust statistical summary plots for the GMU-WFS simulated WD10 in the east and west U.S. for further reference.

3.2.2. Chemistry evaluation

The GMU-WFS demonstrates overall good model agreement with the observed 550 nm aerosol optical depth (AOD; against VIIRS) and the spatial

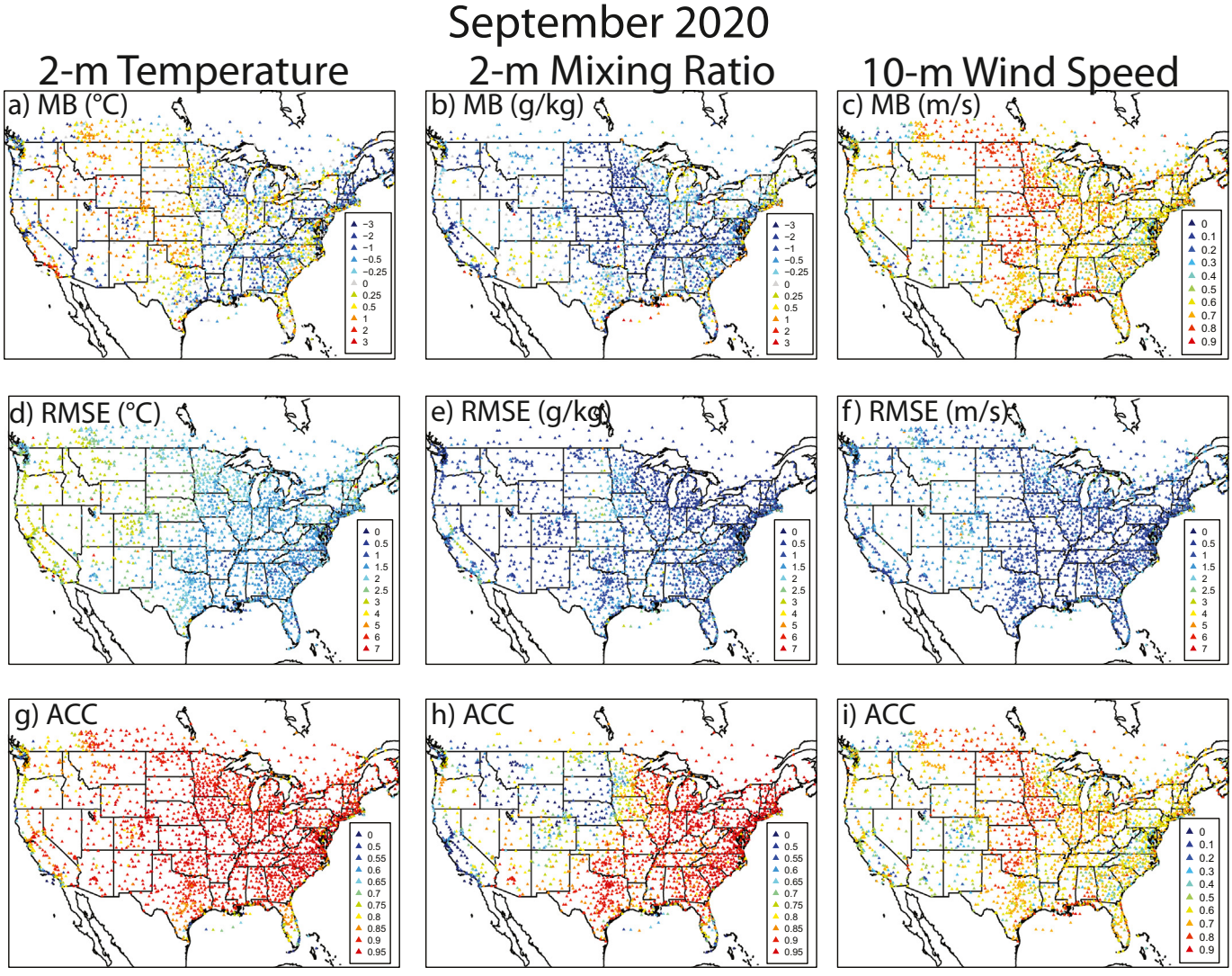

Fig. 2. Average September 2020 spatial a-c) MB, d)-f) RMSE, and g)-i) ACC statistics for the GMU-WFS simulated TEMP2, Q2, and WS10 compared against the MADIS/METAR network.

distribution of near-surface $PM_{2.5}$ concentrations (against the U.S. EPA AirNow Network) for the August–October 2020 ACF period (See Fig. 2 in Li et al., 2021). Overall, the GMU-WFS model demonstrates the ability to reproduce the large-scale wildfire smoke dispersion, especially when the fire is intense; however, the near-surface $PM_{2.5}$ evaluation in Li et al. (2021) is only shown for spatial overlay on September 15, 2020 across relatively wide bracketed $PM_{2.5}$ concentration ranges.

Here we show a more detailed statistical evaluation of the average September 2020 $PM_{2.5}$ and NO_2 concentrations against the AirNow network for the western U.S. (Fig. 3). There are high $PM_{2.5}$ overpredictions (Normalized Mean Bias, NMB ~ 82%; Normalized Mean Error, NME ~ 138%; Index of Agreement, IOA ~ 0.2) near the major ACF fire source regions in September (Fig. 3a). However, the AirNow $PM_{2.5}$ measurement devices may be limited during long-term, extreme BB smoke plume events such as the ACF. In such occurrences, the flow rates may be affected and slow down after a period of time due to a clogged filter, and the response/concentrations may become saturated (https://www.airnow.gov/fires/using-airnow-during-wildfires/). In fact, the GMU-WFS has better model performance for NO_2 concentrations near the major ACF regions, with an overall relatively low NMB and NME (~ −18% and 59%) and high IOA (~ 0.7). While this indeed provides guidance on the model NO_2 performance, we note that standard ground-based NO_x evaluations may involve errors of a factor of two or more due to interferences from other nitrogen species (e.g., NO_y) (Dickerson et al. (2019).

Further comparison of the GMU-WFS against the IMPROVE and CSN near-surface total $PM_{2.5}$ (PM25_TOT), $PM_{2.5}$ sulfate (PM25_SO4), $PM_{2.5}$ nitrate (PM25_NO3), and $PM_{2.5}$ ammonium ion (PM25_NH4) concentrations show generally good agreement for the spatial pattern of higher values near major BB source regions in September 2020 (Fig. 4). While the simulated higher $PM_{2.5}$ values near fire sources are in qualitative good agreement with the location of such observed values (also see Li et al.,

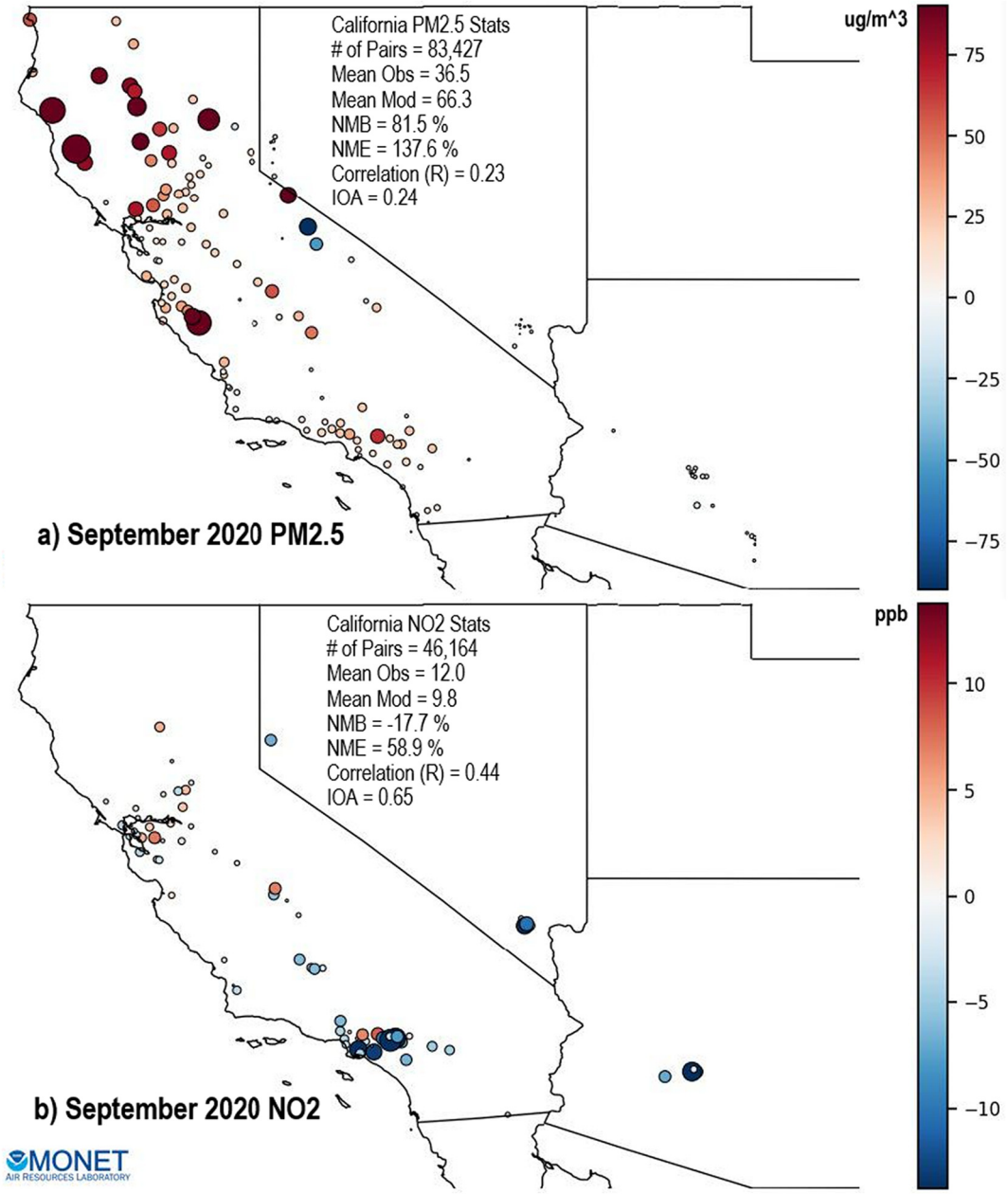

Fig. 3. Average September 2020 AirNow spatial bias (model-observation) evaluation for a) $PM_{2.5}$ (μg m^{-3}), and b) NO_2 (ppb). Monthly average statistics for California are shown in the insert, where NMB = Normalized Mean Bias, NME = Normalized Mean Error, R = Pearson's Correlation Coefficient, and IOA = Index of Agreement.

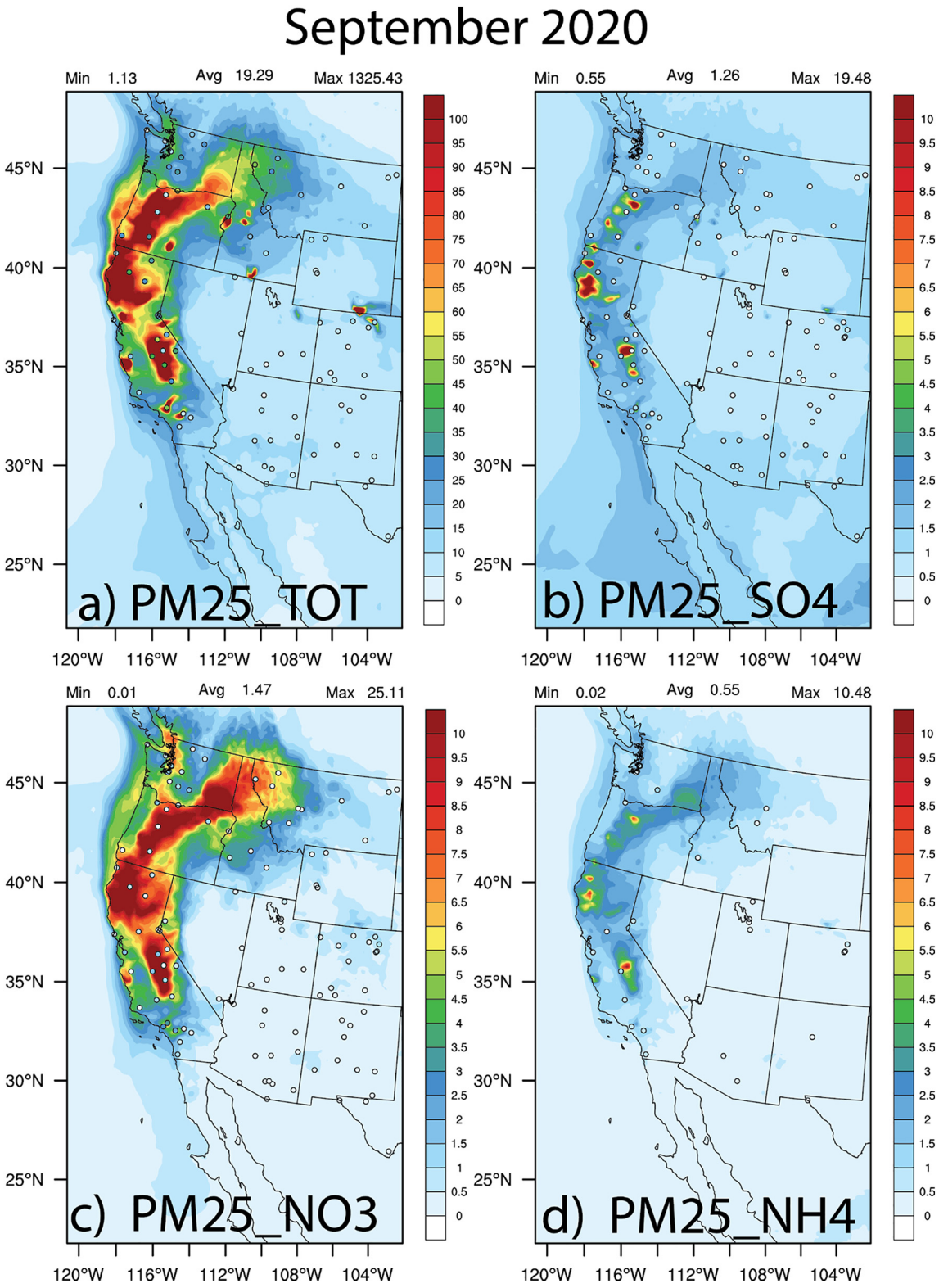

Fig. 4. Combined IMPROVE and CSN spatial overlay comparison for PM25_TOT (IMPROVE only), PM25_SO4 (IMPROVE + CSN), PM25_NO3 (IMPROVE + CSN), and PM25_NH4 (CSN only) averaged over September 2020. The temporal resolution of IMPROVE and CSN networks are 3-day averages.

2021), we note that there is some discrepancy in terms of the simulated $PM_{2.5}$ magnitudes in Fig. 4.

The model results suggest extreme $PM_{2.5}$ concentrations (max >1000 μg m^{-3}) in September, and appear overpredicted compared to the IMPROVE observations (Fig. 4a). The largest contributions to the inorganic $PM_{2.5}$ is from PM25_NO3, then PM25_SO4, and then PM25_NH4, where all components appear to be overpredicted in GMU-WFS. However, we note that there is limited spatial coverage for the CSN PM25_NH4 observations, and similar to the AirNow total $PM_{2.5}$ comparison, extremely high $PM_{2.5}$ concentrations from BB sources may not well be captured by the IMPROVE and CSN measurement devices due to possible instrument saturation. Thus, the AirNow, IMPROVE, and CSN $PM_{2.5}$ observations

may be biased low. However, we also note that the GMU-WFS/GBBEPx spatiotemporal (i.e. once-per-day at 12 × 12 km) resolutions may be limited in accurately capturing the BB emissions that drive the magnitude of $PM_{2.5}$ wildfire plumes in the western U.S. Indeed, there is active development and application of a higher hourly and 3 × 3 km resolution GBBEPx dataset at GMU and NOAA, which has shown to improve September 2020 CMAQ $PM_{2.5}$ predictions compared to the original daily 12 × 12 km GBBEPx emissions in some cases (Jianping Huang/NOAA; personal communication). However, the comparisons shown here are valid in the sense that the 2020 wildfires (e.g. the ACF event) are relatively larger in area compared to the 12 × 12 km horizontal grid resolution of the GMU-WFS. While the evaluation of the BB smoke plumes with "ground

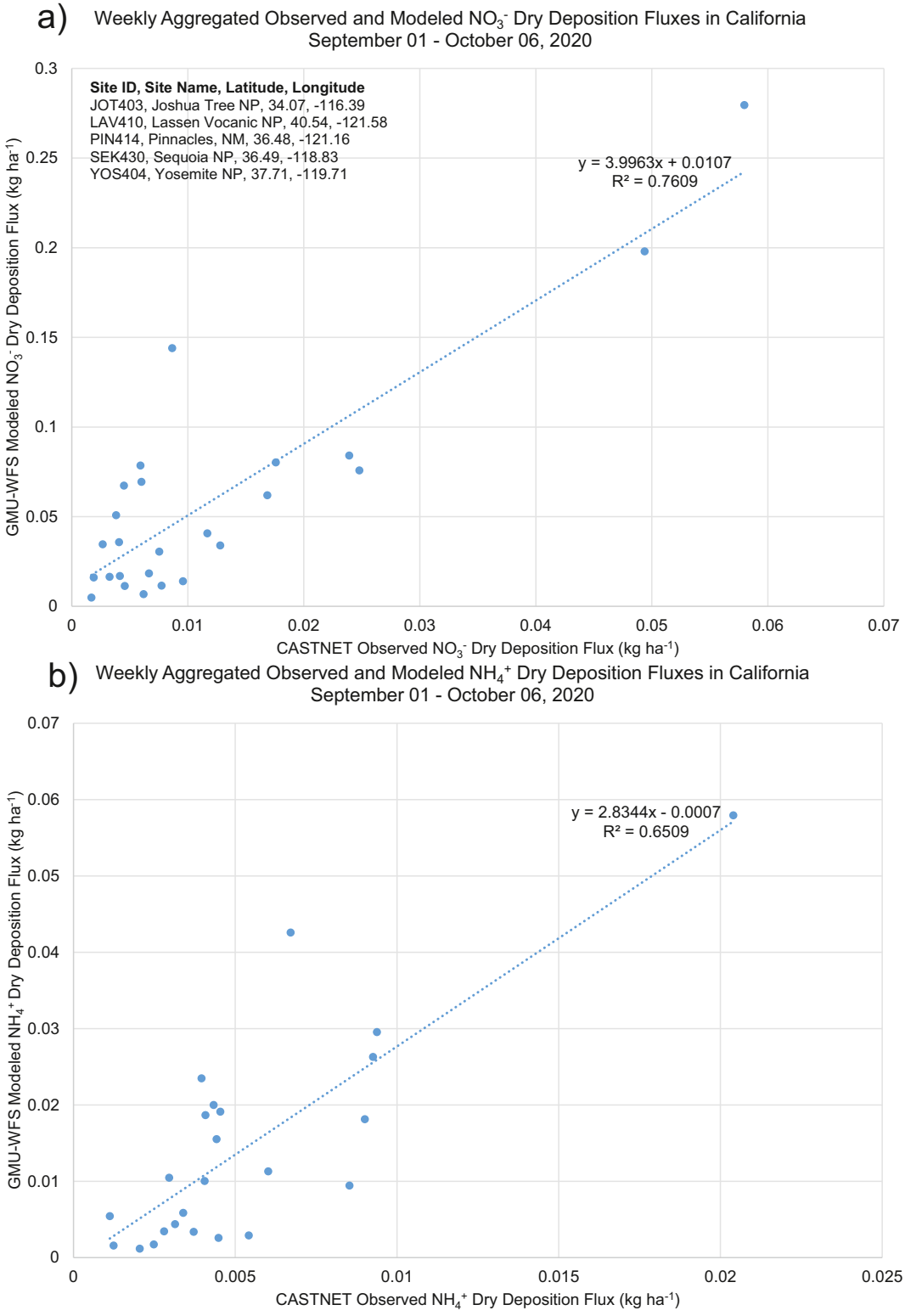

Fig. 5. Weekly aggregated CASTNET observed (x-axis) and GMU-WFS predicted (y-axis) dry deposition fluxes of a) NO_3^- and b) NH_4^+ in California between September 01 and October 06, 2020. The regression lines shown also includes the linear equations for reference. The five CASTNET sites in California are shown in panel a).

truth" data are limited for the 2020 wildfire events, there is confidence that the overall GMU-WFS $PM_{2.5}$ and NO_2 spatial patterns demonstrate skill and agreement with observations here and in Li et al. (2021).

3.2.3. Dry deposition evaluation

While field observations of atmospheric deposition (both dry and wet) are relatively sparser in space and time and subject to larger uncertainties than $PM_{2.5}$ concentrations, we compare weekly aggregated observed CASTNET NO_3^- and NH_4^+ dry deposition against GMU-WFS in California between September 1 and October 6, 2020 (Fig. 5).

The GMU-WFS simulated dry deposition of NO_3^- and NH_4^+ are larger than CASTNET by a factor of ~4 and 3; however, there are overall good agreement in correlation with an R^2 of ~0.76 and 0.65, respectively. Thus, while overpredicted, the good correlations demonstrate skill for the GMU-WFS in predicting the relatively higher dry deposition values during the ACF events in California.

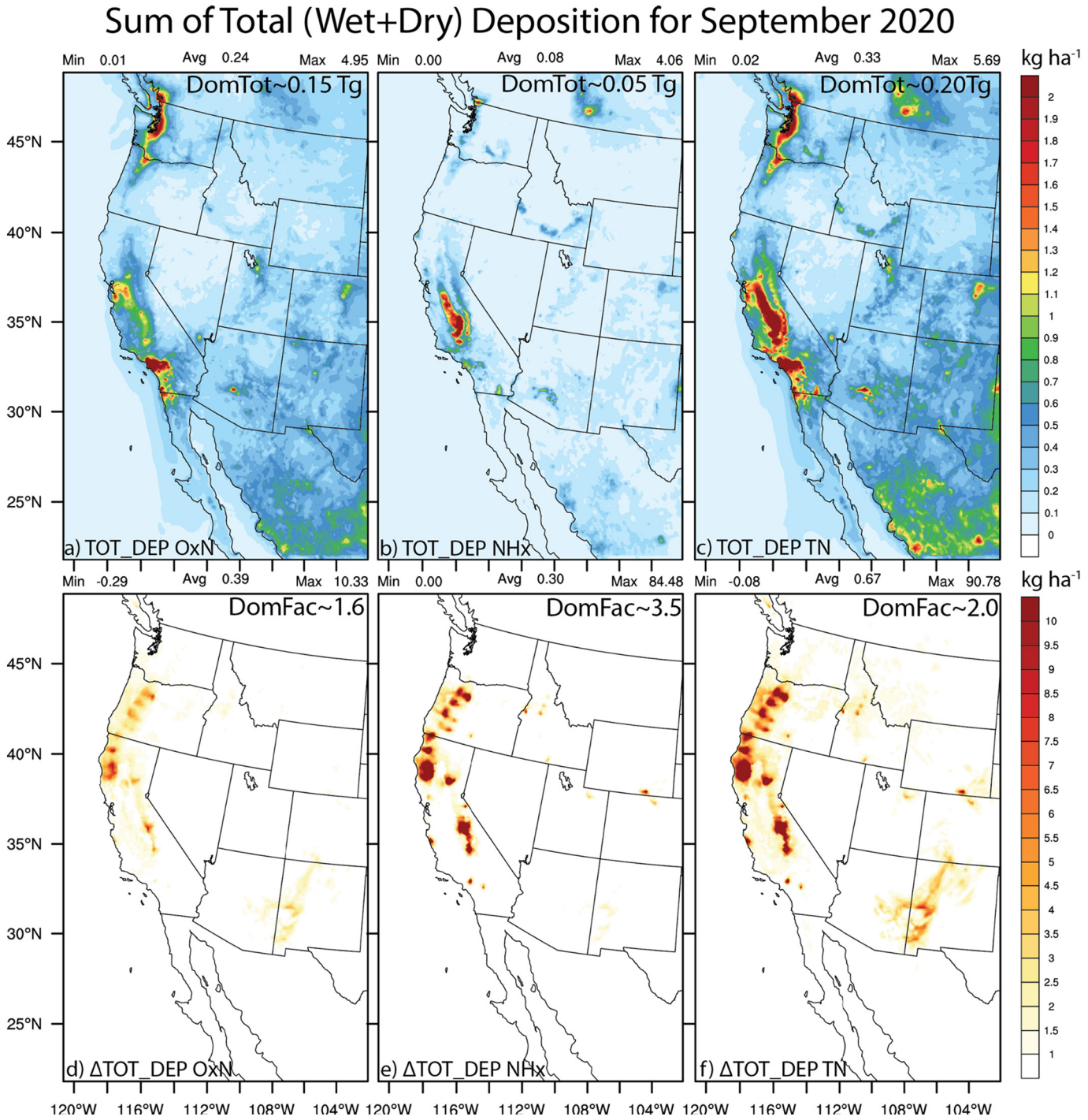

Fig. 6. Sum of September 2020 total (wet and dry) deposition (kg ha^{-1}) for a) oxidized nitrogen (OxN ~ $NO + NO_2 + HNO_3^- + N_2O_5 + ClNO_3 + NO_3^-$), b) reduced nitrogen (NHx ~ $NH_3 + NH_4^+$), and c) total nitrogen (TN = OxN + NHx) species for the NOF case, as well as d)-f) the total deposition changes when including fires (ALLF-NOF). The "DomTot" and "DomFrac" in the upper right corner of the panels represent the western U.S. (> 102°W) NOF total deposition (in Teragrams; Tg) and ALLF fractional deposition increases, respectively.

3.3. Impacts of the 2020 biomass burning emissions on nitrogen deposition

Overall, the highest levels of N deposition in the U.S. are found in the forested areas of California, and are mainly due to dry deposition (Fenn et al., 2012; Bytnerowicz et al., 2016). The no wildfire (NOF) model simulation in our work shows that the oxidized (OxN ~ $NO + NO_2$ + HNO_3^- + N_2O_5 + $ClNO_3$ + NO_3^-), reduced (NHx ~ NH_3 + NH_4^+), and total N (TN = OxN + NHx) deposition (TOT_DEP TN; dry + wet) have September 2020 maxima in the Pacific Northwest and in the central and southern parts of California, which are mainly areas just downstream of major urban centers (e.g., Seattle, San Francisco, and Los Angeles) typical of very high anthropogenic emissions (Fig. 6a-c). Most of the higher N deposition in central and southern California, e.g. the TOT_DEP NHx maximum in the San Joaquin Valley air basin, is due to high dry deposition rates of reactive N species in this region (Fenn et al., 2010; Bytnerowicz et al., 2016). Largely, the N deposition in California is dominated by dry deposition of nitric acid vapor (HNO_3) and NH_3, which are driven by their relative high ambient concentrations and high deposition velocities (Bytnerowicz and Fenn, 1996; Bytnerowicz et al., 2016). While not shown here, these aspects are consistent with the results of the GMU-WFS predictions for the NOF case.

The addition of BB burning emissions in the ALLF case leads to significant additions (ALLF-NOF) of oxidized (ΔTOT_DEP OxN), reduced (ΔTOT_DEP NHx), and total N (ΔTOT_DEP TN) deposition in regions outside the NOF maxima (Fig. 6d-f). Near the vicinity of the extreme NO_x and NH_3 BB emissions (Fig. 1a-c), there are increases in the TOT_DEP TN of up to ~91 kg ha^{-1} (Fig. 6f) that are dominated by reduced N (TOT_DEP NHx; Fig. 6e) in September. There is a factor of 1.6, 3.5, and 2.0 increase in the TOT_DEP OxN, TOT_DEP NHx, and TOT_DEP TN for the entire western U.S. for the ALLF compared to the NOF case. Supporting Fig. S4a-4f show similar spatial plots for all months during the 2020 year, which clearly indicate that the 2020 ACF (August–October) events dominate the TN increases due to fires in the west. While the natural state of aquatic and terrestrial ecosystems in California is one of limited N availability (Bytnerowicz et al., 2016), such large increases in N deposition due to wildfires will have significant ecological effects on California's ecosystems (e.g., nitrogen excess).

3.4. Implications of wildfire-enhanced nitrogen deposition for California ecosystems

The most widespread impacts of N deposition observed in California are shifts in communities of epiphytic lichens (defined as organisms that grow on the surface of a plant) in forests and chaparral/oak woodlands (Bytnerowicz et al., 2016). Epiphytic lichens are among the most sensitive bioindicators of N in forested ecosystems and are particularly responsive to

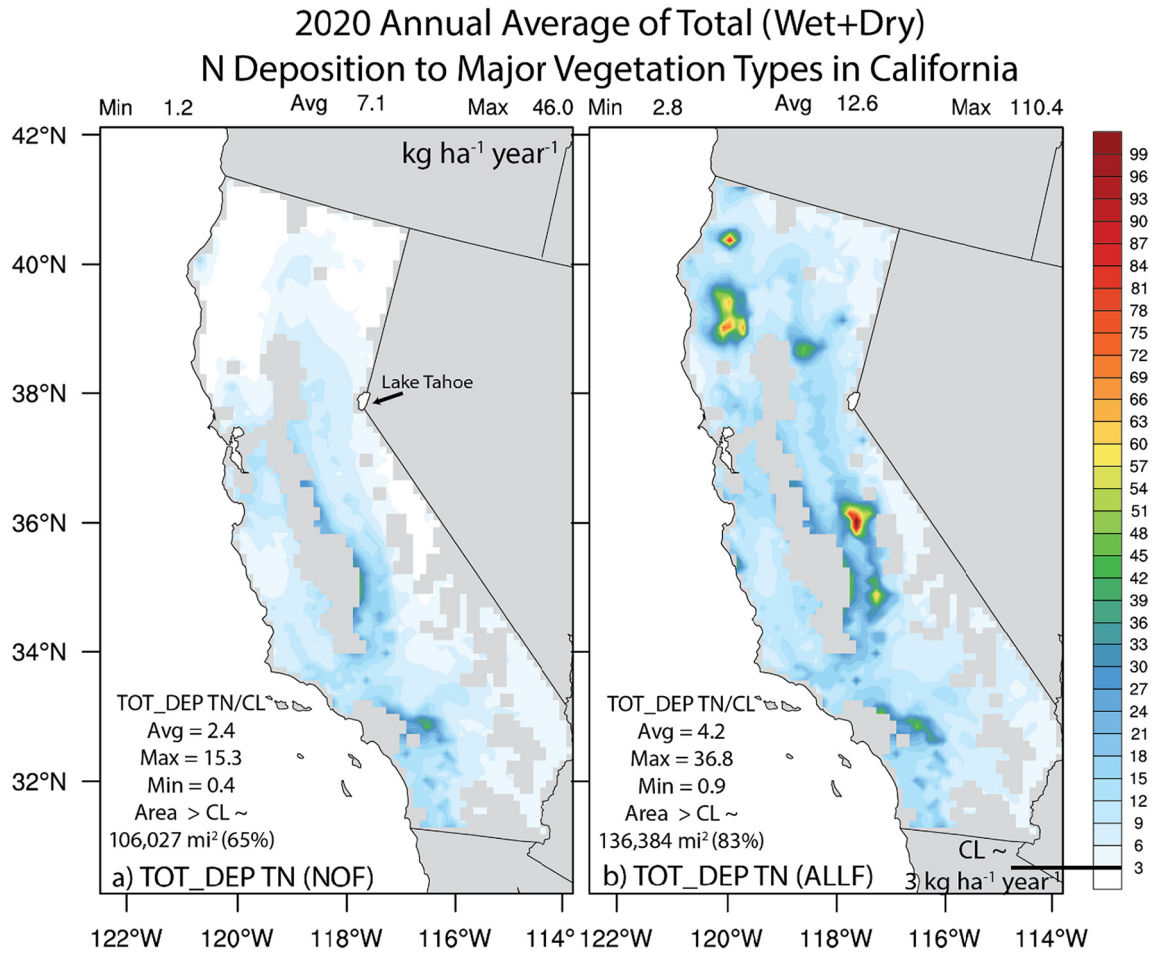

Fig. 7. 2020 Annual average of total (wet and dry) nitrogen (TN = OxN + NHx) species deposition (kg ha^{-1} $year^{-1}$) for the a) NOF and b) ALLF cases. Data within the state of California is shown, and is further masked by the model dominant landuse types that represent a total of 8 major vegetation types including deciduous broadleaf forest, deciduous needle leaf forest, evergreen broadleaf, evergreen needleleaf, other mixed forest, grasslands, shrublands, and savanna from the USGS 24-category land use data used in the simulation. Note that the color scale includes shading (other than white) only for those levels above a low-end Critical Load (CL) ~ 3 kg ha^{-1} $year^{-1}$, above which can result in adverse N deposition effects on lichen communities found in California mixed conifer forests and some scrub species (see Fenn et al., 2008 and Table 7.2 in Bytnerowicz et al., 2016). The insert statistics are the plotted values divided by the CL ~ 3 kg ha^{-1} (i.e., factor of values > CL), the area in square miles of values > CL, and the representative % of the total area of California (~ 163,696 mi^2) in parentheses.

changes in environmental stressors (e.g., forest structure, air quality, and climate), while alleviating the difficulty in separating the effects of air pollutants and deposition from other influences on tree growth (such as soil variations) (Fenn et al., 2008). Consequently, the implementation of lichen-derived Critical Load (CL) thresholds for N deposition can prevent undesired impacts to the broader forest ecosystem (e.g., expansion of invasive species, vegetation change, and biodiversity loss), particularly in areas of exacerbated near-surface ozone pollution levels. Indeed, many areas of California already fall into this category. Oligotrophic species (defined as plants that can live where there aren't many available nutrients) are highly sensitive to atmospheric N, with initial declines in number observed at N deposition levels (i.e. CLs) as low as 3 kg ha^{-1} $year^{-1}$ (Fenn et al., 2008; Bytnerowicz et al., 2016).

In the case of no BB emissions (NOF) during 2020, there are widespread areas of relatively low to moderate TOT_DEP TN to the major vegetation types in California, many of which still exceed the low-end CL of 3 kg ha^{-1} $year^{-1}$ (Fig. 7a). The presence of extreme BB emissions largely due to the ACF events, however, leads to a substantial increase in annual average TOT_DEP TN with an average relative increase of ~78% (from 7.1 to 12.6 kg ha^{-1} $year^{-1}$) to the major vegetation types in California (Fig. 7b). To place this into context, the ~5.5 kg ha^{-1} yr^{-1} increase in TN deposition during 2020 is significantly larger than shown in Koplitz et al. (2021), which estimated that wildland fires contributed 0.2 kg N ha^{-1} yr^{-1} on average across the US during 2008–2012, with maxima up to 1.4 kg N ha^{-1} yr^{-1} in the Northwest. The large increase may be reflective of a significant interannual variability in TOT_DEP TN due to wildfire occurence and severity in the western U.S., where further work is needed to investigate long-term BB emissions trends and impacts on N deposition.

Supporting Fig. S5 (and graphical abstract) shows a similar plot for the TOT_DEP TN/CL ratio for both the NOF and ALLF case. Overall, the average TOT_DEP TN/CL ratio increases from 2.4 (NOF) to 4.2 (ALLF), with an ALLF grid cell maximum of up to ~37 times greater N deposition (at ~110 kg ha^{-1} $year^{-1}$) compared to the low-end CL (Supporting Fig. S5). The enhanced N deposition leads to an increase in area of TOT_DEP TN > CL from 65% to 83% for the major vegetation types relative to the total area of California (~ 163,696 mi^2) (Fig. 7).

The increase in TOT_DEP TN is even larger to mixed forests in the ALLF case, with increases of ~173% when including BB emissions that are about *six times* larger than the lichen-based CL of 3 kg ha^{-1} $year^{-1}$ (Table 3). We note that relatively new research has indicated an even lower CL for U.S. forests of 1.5 kg N ha^{-1} yr^{-1} (Geiser et al., 2021), which suggests that BB in the ALLF would have even larger (i.e., *twelve times* larger) increases in annual average N deposition to California's forests. For grasslands/shrublands/savanna, croplands/pasture, and inland water body land use types, the increases are ~37%, 22%, and 17%, respectively (Table 3).

Here we note that choice of a single, conservatively low CL ~ 3 kg ha^{-1} $year^{-1}$ for all major vegetation types is an approximation, where different CL thresholds based on a range of ecosystem response variables can be applied for a single vegetation type (e.g., mixed forests) or for different vegetation types (e.g., grasslands/shrublands) (see Table 7.2 in Bytnerowicz et al., 2016). Thus, Supporting Figs. S6 and S7 show the range of annual average 2020 TOT_DEP TN/CL ratios for mixed forests across a range of CL thresholds (~ 3, 5, 10, and 17 kg ha^{-1} $year^{-1}$) from Bytnerowicz et al. (2016) and for grasslands/shrublands (CL ~ 6 kg ha^{-1} $year^{-1}$) in California. The enhanced N deposition due to the ACF fire events leads to a wide range of profound ecosystem effects that can vary spatially for different vegetation across California; however, the largest N deposition increases due to fires are clearly due to the mixed forests types (compare Fig. S6 and S7).

There are also increases in TOT_DEP TN to California's inland water bodies due to BB burning (~ 17%; Table 3), where high nitrate ion (NO_3^-) concentrations in surface waters are harmful pollution. Increases in N deposition to Lake Tahoe have led to doubling in the mean annual primary productivity, decreases in Secchi disk transparency (i.e., water clarity), and increases in the eutrophic to mesotrophic diatom *Fragilaria crotonensis* (common araphid species in temperate, mesotrophic lakes of North America; see Fenn et al., 2003 and references within). High NO_3^- deposition is known to induce toxic effects on freshwater biota (Fenn et al., 2003), and there are recent reports of beneficial decreases in NO_3^- concentrations in surface waters that are primarily attributed to decreases in the emissions of precursor air pollutants (e.g., NO_x; Austnes et al., 2018).

Extreme wildfires and BB emissions can detrimentally counteract the progress made in reducing the total NO_3^- deposition in California. The ~17% increase in N deposition to inland water bodies mainly consists of Lake Tahoe, which is California's largest lake (area ~ 191 mi^2) expanding across the border into Nevada (see Fig. 7a). In addition to well documented reductions in water clarity and increased algal growth, Lake Tahoe has also experienced shifts in diatom communities due to N enrichment (see Table 2 in Fenn et al., 2003 and references found within). More detailed studies are needed on the impacts of large to extreme wildfire events and BB emissions on N deposition to inland water bodies in California and the western U.S.

Table 3
2020 Annual average of total (wet and dry) nitrogen (TN = OxN + NHx) species deposition (kg ha^{-1} $year^{-1}$) for different combined land use types[a] in California.

Land Use Types	NOF	ALLF	Relative (%) Change
Major Vegetation Types (Fig. 5)	7.1	12.6	77.5
Mixed Forests	6.2	16.9	172.6
Grassland/Shrubland/Savanna	7.6	10.4	36.8
Croplands/Pasture	18.0	22.1	22.8
Inland Water Bodies[b]	2.3	2.7	17.4

[a] Combined USGS-24 Category land use types: All Major Vegetation = Mixed Forests + Grassland/Shrubland/Savanna; Mixed Forests = 11–15; Grassland/Shrubland/Savanna = 7–10; Croplands and Pasture = 2–6; Inland Water Bodies/Lake Tahoe Only = 16.

[b] Lake Tahoe (labeled in Fig. 7) values include those grid cells across both California and Nevada.

4. Summary and discussion

In this work, we use satellite-based observations and modeling to quantify the contributions of biomass burning (BB) to the total emissions, and the impacts of such BB emissions on nitrogen (N) deposition in the western U.S. during 2020 that included a historic wildfire season (e.g., August–October). We find that during the 2020 wildfire season BB contributes significantly to the total emissions, with a satellite-derived fraction of NH_3 to the total reactive N emissions (range ~ 15%–52%; mean ~ 37%; median ~ 40%) that is in the range of previous aircraft observations (Lindaas et al., 2021). During the peak of the western August Complex Fires (ACF) in September, BB contributed to ~55% (for contiguous U.S.) and ~ 83% (for western U.S.) of the total NO_x and NH_3 emissions.

Previous evaluation of the George Mason University-Wildfire Forecast System (GMU-WFS) shows overall good model performance of the novel Blended Global Biomass Burning Emissions Product (GBBEPx) with the Sofiev plume rise scheme, as well as the ability of the model to reproduce the large-scale smoke transport and near-surface total $PM_{2.5}$ concentration ranges across the U.S. from August–October 2020 (Li et al., 2020, 2021). Further evaluation here of the simulated meteorology demonstrates that the GMU-WFS is near or within reported model bias and error performance benchmarks. Evaluation of the GMU-WFS simulated near-surface $PM_{2.5}$ and associated sulfate, nitrate, and ammonium ion composition against the AirNow, CSN, and IMPROVE networks, as well as evaluation of the simulated dry deposition against CASTNET in this work identifies possible model overpredictions; however, potential instrument issues and measurement uncertainties at extremely high wildfire-related $PM_{2.5}$ concentrations are possible.

5. Conclusions

The extreme 2020 BB emissions lead to significant contributions to the total N deposition for different ecosystems in California, with ~ a 78% relative increase (from 7.1 to 12.6 kg ha^{-1} $year^{-1}$) in average deposition to the major vegetation types (mixed forests + grasslands/shrublands/savanna) compared to the GMU-WFS simulations without BB emissions. To place into context, these increases are much larger than the 5 year annual average increases in N deposition reported for the 2008–2012 period (Koplitz et al., 2021). For mixed forest types only, the relative N deposition increases (from 6.2 to 16.9 kg ha^{-1} $year^{-1}$) are even larger at ~173%. Such large N deposition due to extreme BB emissions are much (~6-12 times) larger than low-end critical load thresholds for major vegetation types (e.g., 1.5-3 kg ha^{-1} $year^{-1}$; Fenn et al., 2008; Bytnerowicz et al., 2016; Geiser et al., 2021), and may result in adverse N deposition effects across larger areas of lichen communities found in California's mixed conifer forests. Indeed, there are persistent feedbacks of long-term fire suppression, increased fuel consumption, climate change, drought stress, invasive species outbreaks, extreme mega- and gigafire events (e.g., the 2020 ACF events in this study), and excess N deposition that have already affected and will continue to affect the vigor, resilience, and sustainability of U.S. forests.

CRediT authorship contribution statement

Patrick C. Campbell: Conceptualization, Methodology, Software, Data curation, Visualization, Investigation, Writing – original draft. **Daniel Tong:** Supervision, Project administration, Software, Data curation, Writing – review & editing. **Rick Saylor:** Supervision, Project administration, Software, Data curation, Writing – review & editing. **Yunyao Li:** Methodology, Software, Data curation, Writing – review & editing. **Siqi Ma:** Methodology, Software, Data curation. **Xiaoyang Zhang:** Data curation. **Shobha Kondragunta:** Data curation. **Fangjun Li:** Data curation.

Declaration of competing interest

The authors declare that they have no known competing financial interests or personal relationships that could have appeared to influence the work reported in this paper.

Acknowledgments

This study was co-funded by the National Oceanic and Atmospheric Administration, the University of Maryland, and George Mason University under the Cooperative Institute for Satellite Earth System Studies (CISESS).

The MADIS/METAR data for 09/01/2020–09/30/2020 is provided by the NOAA/NCEP Central Operations website, and can be downloaded from https://madis-data.ncep.noaa.gov/. The U.S. EPA AirNow data for 09/01/2020–09/30/2020 was provided by the AirNow Application Programming Interface (API) (more information found at: https://docs.airnowapi.org/), and can be downloaded from https://files.airnowtech.org/?prefix=airnow/2020/. The IMPROVE data was made available from the Federal Land Manager Environmental Database (FED-2020) IMPAER data for 09/01/2020–09/30/2020, and can be obtained from the FED website at https://views.cira.colostate.edu/fed (previously obtained on 01/25/2022). The CSN data was made available from the FED-2020 EPACSN data for 09/01/2020–09/30/2020, and can be obtained from the FED website at https://views.cira.colostate.edu/fed (previously obtained on 01/25/2022). The CASTNET data for 09/01/2020–10/06/2020 was made available from the U.S. EPA, and can be obtained from the U.S. EPA CASTNET website at https://java.epa.gov/castnet/. The GBBEPx data can be downloaded from https://satepsanone.nesdis.noaa.gov/pub/FIRE/GBBEPx-V3/ and the GMU-WFS/CMAQ model results can be downloaded from: http://air.csiss.gmu.edu/yli/paper_data/.

Appendix A. Supplementary data

Supplementary data to this article can be found online at https://doi.org/10.1016/j.scitotenv.2022.156130.

References

Appel, K.W., Gilliam, R.C., Davis, N., Zubrow, A., Howard, S.C., 2011. Overview of the atmospheric model evaluation tool (amet) v1.1 for evaluating meteorological and air quality models. Environ. Model. Softw. 26, 434–443. https://doi.org/10.1016/j.envsoft.2010.09.007.

Austnes, K., Aherne, J., Arle, J., Čičendajeva, M., Couture, S., Fölster, J., Garmo, O., Hruška, J., et al., 2018. Regional Assessment of the Current Extent of Acidification of Surface Waters in Europe And North America. Norwegian Institute for Water Research.

Baker, B., Pan, L., 2017. Overview of the Model and Observation Evaluation Toolkit (MONET) version 1.0 for evaluating atmospheric transport models. Atmosphere 8, 210. https://doi.org/10.3390/atmos8110210.

van den Berg, L.J., Jones, L., Sheppard, L.J., Smart, S.M., Bobbink, R., Dise, N.B., Ashmore, M.R., 2015. Evidence for differential effects of reduced and oxidised nitrogen deposition on vegetation independent of nitrogen load. 2016 Jan. Environ. Pollut. 208 (Pt B), 890–897. https://doi.org/10.1016/j.envpol.2015.09.017. Epub 2015 Oct 21. PMID: 26476695.

Bytnerowicz, A., Padgett, P.E., Parry, S.D., Fenn, M.E., Arbaugh, M.J., 2001. Concentrations, deposition, and effects of nitrogenous pollutants in selected california ecosystems. Optimizing Nitrogen Management in Food and Energy Production and Environmental Protection: Proceedings of the 2nd International Nitrogen Conference on Science and Policy. https://doi.org/10.1100/tsw.2001.395.

Bytnerowicz, A., Fenn, M., 1996. Nitrogen deposition in California forests: a review. Environ. Pollut. 92, 127–146.

Bytnerowicz, A., Fenn, M.E., Allen, E.B., Cisneros, R., 2016. Ecologically relevant atmospheric chemistry. Chapter 7 In: Zavaleta, E., Mooney, H.A. (Eds.), Ecosystems of California. University of California Press, Berkeley, Calif., pp. 107–128.

California Department of Forestry and Fire Protection (CAL FIRE), 2020. 2020 fire season. Retrieved from. https://www.fire.ca.gov/incidents/2020/.

Cascio, W.E., 2018. Wildland fire smoke and human health. Sci. Total Environ. 624, 586–595. https://doi.org/10.1016/j.scitotenv.2017.12.086.

Darmenov, A., da Silva, A., 2013. In: Suarez, M.J. (Ed.), The Quick Fire Emissions Dataset (QFED) - Documentation of Versions 2.1, 2.2 And 2.4. Technical Report Series on Global Modeling And Data Assimilation. Vol. 32.

Dickerson, R.R., Anderson, D.C., Ren, X., 2019. On the use of data from commercial NOx analyzers for air pollution studies. Atmos. Environ. 215. https://doi.org/10.1016/j.atmosenv.2019.116873.

Fahey, K.M., Carlton, A.G., Pye, H.O.T., Baek, J., Hutzell, W.T., Stanier, C.O., et al., 2017. A framework for expanding aqueous chemistry in the Community Multiscale Air Quality (CMAQ) model version 5.1. Geosci. Model Dev. 10, 1587–1605. https://doi.org/10.5194/gmd-10-1587-2017.

Fenn, M.E., Poth, M.A., Schilling, S.L., Grainger, D.B., 2000. Throughfall and fog deposition of nitrogen and sulfur at an N-limited and N-saturated site in the San Bernardino Mountains, southern California. Can. J. For. Res. 30 (9), 1476–1488. https://doi.org/10.1139/x00-076.

Fenn, M.E., Baron, J.S., Allen, E.B., Rueth, H.M., Nydick, K.R., Geiser, L., Bowman, W.D., Sickman, J.O., Meixner, T., Johnson, D.W., Neitlich, P., 2003. Ecological effects of nitrogen deposition in the western United States. BioScience 53 (4), 404–420. https://doi.org/10.1641/0006-3568(2003)053[0404:EEONDI]2.0.CO;2.

Fenn, M.E., Jovan, S., Yuan, F., Geiser, L., Meixner, T., Gimeno, B.S., 2008. Empirical and simulated critical loads for nitrogen deposition in California mixed conifer forests. Environ. Pollut. 155, 492–511. https://doi.org/10.1016/j.envpol.2008.03.019.

Fenn, M.E., Allen, E.B., Weiss, S.B., Jovan, S., Geiser, L., Tonnesen, G.S., Johnson, R.F., Rao, L.E., Gimeno, B.S., Yuan, F., Meixner, T., Bytnerowicz, A., 2010. Nitrogen critical loads and management alternatives for N-impacted ecosystems in California. J. Environ. Manag. 91, 2404–2423.

Fenn, M.E., Bytnerowicz, A., Liptzin, D., 2012. Nationwide maps of atmospheric deposition are highly skewed when based solely on wet deposition. Bioscience 62, 621.

Geiser, L.H., Root, H., Smith, R.J., Jovan, S.E., St. Clair, L., Dillman, K.L., 2021. Lichen-based critical loads for deposition of nitrogen and sulfur in US forests. Environ. Poll. 291, 118187. https://doi.org/10.1016/j.envpol.2021.118187.

Geiser, Linda H., Jovan, Sarah E., Glavich, Doug A., Porter, Matthew K., 2010. Lichen-based critical loads for atmospheric nitrogen deposition in Western Oregon and Washington forests, USA. Environ. Pollut. 158, 2412–2421. https://doi.org/10.1016/j.envpol.2010.04.001.

Johnston, F., Henderson, S., Chen, Y., Randerson, J., Marlier, M., DeFries, R., et al., 2012. Estimated global mortality attributable to smoke from landscape fires. Environ. Health Perspect. 120 (5), 695–701. https://doi.org/10.1289/ehp.1104422.

Koplitz, S., Chris Nolte, R., Sabo, C., Clark, K., Horn, R.Thomas, Newcomer-Johnson, T., 2021. The contribution of wildland fire emissions to deposition in the U S: implications for tree growth and survival in the Northwest. Environ. Res. Lett. 16 (2), 024028. https://doi.org/10.1088/1748-9326/abd26e.

Lake Michigan Air Directors Consortium (LADCO), 2018. 2016 Weather Research and Forecasting (WRF) modeling protocol for the LADCO states. Wisconsin Department of Natural Resources. https://www.ladco.org/wp-content/uploads/Modeling/2016/WRF/LADCO_WRF2016_ModelingProtocol_Final.pdf. (Accessed 5 June 2022).

Li, Y., Tong, D.Q., Ngan, F., Cohen, M.D., Stein, A.F., Kondragunta, S., et al., 2020. Ensemble PM2.5 forecasting during the 2018 Camp Fire event using the HYSPLIT transport and

dispersion model. J.Geophys.Res.Atmos. 125, e2020JD032768. https://doi.org/10.1029/2020JD032768.

Li, Y., Tong, D., Ma, S., Zhang, X., Kondragunta, S., Li, F., Saylor, R., 2021. Dominance of wildfires impact on air quality exceedances during the 2020 record-breaking wildfire season in the United States. Geophys. Res. Lett. 48, e2021GL094908. https://doi.org/10.1029/2021GL094908.

Lindaas, J., Pollack, I.B., Garofalo, L.A., Pothier, M.A., Farmer, D.K., Kreidenweis, S.M., et al., 2021. Emissions of reactive nitrogen from Western U.S. wildfires during summer 2018. J. Geophys. Res. Atmos. 125, e2020JD032657. https://doi.org/10.1029/2020JD032657.

Liu, Y., Austin, E., Xiang, J., Gould, T., Larson, T., Seto, E., 2021. Health impact assessment of the 2020 Washington State wildfire smoke episode: excess health burden attributable to increased PM2.5 exposures and potential exposure reductions. GeoHealth 5, e2020GH000359. https://doi.org/10.1029/2020gh000359.

Luecken, D.J., Yarwood, G., Hutzell, W.H., 2019. Multipollutant of ozone, reactive nitrogen and HAPs across the continental US with CMAQ-CB6. Atmos. Environ. 201, 62–72. https://doi.org/10.1016/j.atmosenv.2018.11.060.

Matthias, V., Arndt, Jan A., Aulinger, Armin, Bieser, Johannes, Denier, Hugo, van der Gon, Richard, Kranenburg, Jeroen Kuenen, Neumann, Daniel, Pouliot, George, Quante, Markus, 2018. Modeling emissions for three-dimensional atmospheric chemistry transport models. J. Air Waste Manag. Assoc. 68 (8), 763–800. https://doi.org/10.1080/10962247.2018.1424057.

Miller, J., Safford, H., Crimmins, M., Thode, A., 2009. Quantitative evidence for increasing forest fire severity in the Sierra Nevada and Southern Cascade Mountains, California and Nevada, USA. Ecosystems 12, 16–32. https://doi.org/10.1007/s10021-008-9201-9.

National Emissions Inventory Collaborative, 2019. 2016v1 emissions modeling platform. Retrieved from. http://views.cira.colostate.edu/wiki/wiki/10202.

O'Neill, S.M., Diao, M., Raffuse, S., Al-Hamdan, M., Barik, M., Jia, Y., et al., 2021. A multi-analysis approach for estimating regional health impacts from the 2017 Northern California wildfires. J. Air Waste Manag. Assoc. 71 (7), 791–814. https://doi.org/10.1080/10962247.2021.1891994.

Pye, H.O.T., Luecken, D.J., Xu, L., Boyd, C.M., Ng, N.L., Baker, K.R., et al., 2015. Modeling the current and future roles of particulate organic nitrates in the southerneastern United States. Environ.Sci.Technol. 49 (24), 14195–14203. https://doi.org/10.1021/Acs.est.5b03738.

Reid, C.E., Brauer, M., Johnston, F.H., Jerrett, M., Balmes, J.R., Elliott, C.T., 2016. Critical review of health impacts of wildfire smoke exposure. Environ. Health Perspect. 124, 1334–1343. https://doi.org/10.1289/ehp.1409277.

Skamarock, W.C., Klemp, J.B., Dudhia, J., Gill, D.O., Liu, Z., Berner, J., et al., 2019. A Description of the Advanced Research WRF Version 4. NCAR, p. 145.

Sofiev, M., Ermakova, T., Vankevich, R., 2012. Evaluation of the smoke-injection height from wild-land fires using remote-sensing data. Atmos. Chem. Phys. 12 (4), 1995–2006. https://doi.org/10.5194/acp-12-1995-2012.

United States Environmental Protection Agency, 2020. CMAQ (Version 5.3.2)[Software]. https://doi.org/10.5281/zenodo.4081737. Retrieved From.

Westerling, A.L., Hidalgo, H.G., Cayan, D.R., Swetnam, T.W., 2006. Warming and earlier spring increase western US forest wildfire activity. Science 313, 940–943. https://doi.org/10.1029/2003EO490001.

Xu, L., Pye, H.O.T., He, J., Chen, Y.L., Murphy, B.N., Ng, N.L., 2018. Experimental and model estimates of the contributions from biogenic monoterpenes and sesquiterpenes to secondary organic aerosol in the southeastern United States. Atmos. Chem. Phys. 18, 12613–12637. https://doi.org/10.5194/acp-18-12613-2018.

Zhang, X., Kondragunta, S., Ram, J., Schmidt, C., Huang, H.-C., 2012. Near-real-time global biomass burning emissions product from geostationary satellite constellation. J. Geophys.Res.Atmos. 117 (D14). https://doi.org/10.1029/2012JD017459.

Zhang, X., Kondragunta, S., Roy, D.P., 2014. Interannual variation in biomass burning and fire seasonality derived from geostationary satellite data across the contiguous United States from 1995 to 2011. J.Geophys.Res.Biogeosci. 119 (6), 1147–1162. https://doi.org/10.1002/2013JG002518.